THE JOURNAL OF PHYSICAL CHEMISTRY B
A JOURNAL OF THE AMERICAN CHEMICAL SOCIETY

pubs.acs.org/JPCB

Article

Hydrophobic Gating and 1/*f* Noise of the Anthrax Toxin Channel

Goli Yamini, Subbarao Kanchi, Nnanya Kalu, Sanaz Momben Abolfath, Stephen H. Leppla, K. Ganapathy Ayappa, Prabal K. Maiti, and Ekaterina M. Nestorovich*

Cite This: *J. Phys. Chem. B* 2021, 125, 5466−5478

Read Online

ACCESS | Metrics & More | Article Recommendations | Supporting Information

ABSTRACT: "Pink" or 1/*f* noise is a natural phenomenon omnipresent in physics, economics, astrophysics, biology, and even music and languages. In electrophysiology, the stochastic activity of a number of biological ion channels and artificial nanopores could be characterized by current noise with a 1/*f* power spectral density. In the anthrax toxin channel (PA_{63}), it appears as fast voltage-independent current interruptions between conducting and nonconducting states. This behavior hampers potential development of PA_{63} as an ion-channel biosensor. On the bright side, the PA_{63} flickering represents a mesmerizing phenomenon to investigate. Notably, similar 1/*f* fluctuations are observed in the channel-forming components of clostridial binary C2 and iota toxins, which share functional and structural similarities with the anthrax toxin channel. Similar to PA_{63}, they are evolved to translocate the enzymatic components of the toxins into the cytosol. Here, using high-resolution single-channel lipid bilayer experiments and all-atom molecular dynamic simulations, we suggest that the 1/*f* noise in PA_{63} occurs as a result of "hydrophobic gating" at the ϕ-clamp region, the phenomenon earlier observed in several water-filled channels "fastened" inside by the hydrophobic belts. The ϕ-clamp is a narrow "hydrophobic ring" in the PA_{63} lumen formed by seven or eight phenylalanine residues at position 427, conserved in the C2 and iota toxin channels, which catalyzes protein translocation. Notably, the 1/*f* noise remains undetected in the F427A PA_{63} mutant. This finding can elucidate the functional purpose of 1/*f* noise and its possible role in the transport of the enzymatic components of binary toxins.

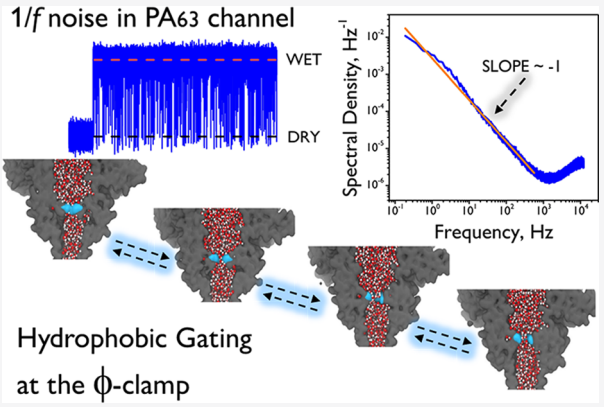

INTRODUCTION

From the simplest molecular processes to the most complex level of cell, tissue, organ, organism and population dynamics, noise runs throughout the living world.[1,2] Conventionally, noise is assumed to be disruptive and consequently considered an unwanted process that must be removed by filtering or other type of signal processing in order to refine the "useful" signal. Yet, the history of how noise development has led to solving great problems in science and technology, where it has served as a rich source of constructive information about the systems, is fascinating.[3] Instead of viewing the fluctuations observed in nature as a nuisance perplexing the experimental measurements, modern quantitative biology considers noise as an essential part of system performance, deserving independent examination.[1,2] At the molecular level of membrane-spanning protein ion channels and artificial nanopores, ion current noise analysis has been successfully used to investigate a variety of natural and engineered transport systems, starting from single polymer sensing[4,5] and ending with commercially available rapid DNA sequencing devices.[6] This approach is largely based on the remarkable ability to observe the transitions between the conducting and nonconducting (or partially conducting) states of single ion channels[7] (the so-called *channel noise*). On the flip side, the same principle is used to explore stochastic ion-channel gating, which plays a fundamental physiological role in neuronal cell excitability.[8−10]

Ion-channel noise can have diverse forms originating from multiple sources, external or internal. One of the long-standing problems in the ion nanopore field is the origin of pink (1/*f* or flicker) noise,[11−17] which was detected in biological ion channels[18−22] and in synthetic nanopores.[23,24] The pink noise has power spectral densities proportional to ~1/*f*, where *f* is the frequency, over a large range of frequencies. In this study, we explore a distinct current noise pattern exhibited by the oligomeric channel-forming component of the binary anthrax toxin channel, protective antigen (PA_{63}), which has evolved to translocate the two other toxin components, lethal factor (LF) and edema factor (EF), into the cytosol. The 2.9 Å cryo-EM imaging of PA_{63} (Figure S1A) revealed a beautiful and stable

Received: November 21, 2020
Revised: May 6, 2021
Published: May 20, 2021

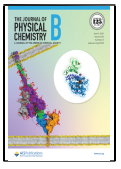

"flower on a stem" structure of the anthrax toxin channel.[25] However, the reality is more complex. The intricate kinetic behavior of the channel, including voltage gating (Figure S1B–D), two open conductance states (*max* and *main*) (Figure S1B), two types of insertion (Figure S1B,C), and intense flickering between open and closed states (Figure S1E) described as the $1/f$ noise process[27] (Figure S1F), makes PA_{63} one of the most puzzling membrane channels to investigate.

Here, using high-resolution single-channel lipid bilayer measurements and all-atom molecular dynamics simulations, we provide the first experimental evidence that the $1/f$ noise in ion channels could be caused by the phenomenon known as hydrophobic gating.[26−32] In PA_{63}, the process is generated at the ϕ-clamp, which is a narrow hydrophobic ring with opposing F427 residues, critical for LF and EF translocation.[33] The flicker noise was also observed with the channel-forming components of the binary C2 toxin of *Clostridium botulinum*[34] and iota toxin of *Clostridium perfringens*[35] but not with the membrane-perforating α-hemolysin of *Staphylococcus aureus*[36] and epsilon toxin of *C. perfringens*.[37] Because the flicker noise manifestation concurs with the translocase activity of the channel-forming components of the binary anthrax, C2, and iota toxins, which contain narrow lumen-exposed aromatic passageways formed by seven phenylalanine residues at positions 427, 428, and 454, respectively[38−40] (described above as the ϕ-clamp), we hypothesize that dewetting of the ϕ-clamp region plays a central role in the intracellular uptake of their enzymatic components.

RESULTS

$1/f$ Noise in PA_{63} Conductance Is Independent of Voltage, Electrolyte Concentration, pH, and Lipid Composition. Typical examples of the ion current through a single PA_{63} channel taken at 100, 50, and −20 mV are given in Figure 1A. Fast fluctuations between the completely open and closed states of the channel are seen at all voltages. Power spectral density plots[41] of these fluctuations in the $\log_{10}$–$\log_{10}$ scale, analyzed at a wide (−20 to +100 mV) range of applied transmembrane voltages, can be fitted by a negative linear dependence with the slope equal to ∼(−1) at $f <$ (100−2000) Hz (depending on the applied voltage) (Figure 1B). A dwell residence time histogram example of the flickering events is given in ref 22 (Figure 4A, a solid curve). This is characteristic of $1/f$ noise behavior. The $1/f$ fluctuations were highly reproducible between the individual channels and their frequency, and the open- and closed-state probabilities were time-independent.[42] In Figure 1C, we show that in PA_{63} the $1/f$ current fluctuations, measured at 10 Hz, scale as the voltage squared, i.e., d log S(10Hz)/d log $V \approx 2$. Accordingly, when the power spectra shown in Figure 1B were normalized by dividing by the squared channel mean current at 10 Hz, the spectra overlapped (Figure 1D). This finding indicates that in PA_{63} the $1/f$ conductance fluctuations are voltage-independent. The $1/f$ noise in the PA_{63} current has been observed at a variety of experimental conditions, such as different bathing electrolyte concentrations (Figure 2), compositions (Figure 3), and pH (Figure S2).[43] It has been detected in PA_{63} type I and type II insertions[22] (Figure S3), in both octameric[44,45] and heptameric[46] PA_{63} channels (Figure S4), when PA_{63} was reconstituted in bilayer membranes made using different neutral and negatively charged, lamellar and nonlamellar lipids[47] (Figure 4). All these factors do not appear to have

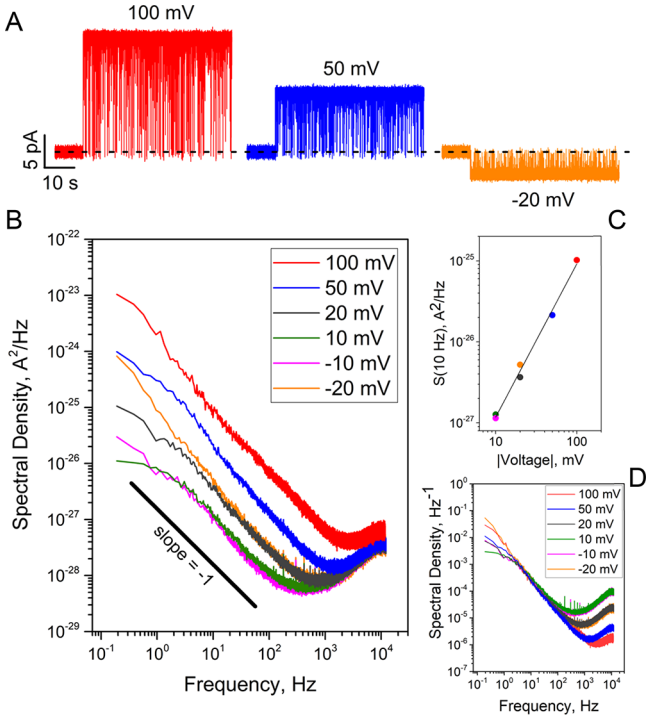

Figure 1. $1/f$ noise in PA_{63} conductance is voltage-independent. (A) Typical tracks of ion current through a single PA_{63} channel in main state insertion,[22] recorded at 100, 50, and −20 mV. The dashed line represents a zero-current level. The current tracks were filtered over 1 ms. (B) In the log−log scale, the power spectral densities of PA_{63} $1/f$ noise current fluctuations have comparable slopes, which are close to −1, when taken at different transmembrane voltages (−20 to +100 mV) at a wide range of frequencies, $f <$ (100−2000) Hz (the lower limit is determined by the voltage magnitude). (C) In the log−log scale, power spectral densities of $1/f$ noise calculated as averages, at 10 Hz, scale as the applied voltage squared. (D) When normalized, dividing by the mean current squared, the power spectral density of $1/f$ noise overlaps at 0.1−100 Hz for all the applied voltages. The measurements were performed in 1 M KCl at pH 6.0 (5 mM MES).

any substantial effect on the frequency, duration, and amplitude of the $1/f$ fluctuations. We have also previously shown that the $1/f$ process is independent of the supporting electrolyte, bilayer membrane lipid, and PA_{63} protein solution purity[42] and therefore, in contrast to earlier suggestions, is not caused by the presence of "a contaminant small molecule, buffer ion, or peptide" that "momentarily binds and occupies the ϕ-clamp".[48]

$1/f$ Noise as a Universal Property of the Bacterial Binary PA_{63}, C2IIa, and Ib Channels. It is noteworthy that identical $1/f$ current fluctuations were also detected using two clostridial binary bacterial toxin channels, C2IIa and Ib, the channel-forming component of the *C. botulinum* C2 toxin and *C. perfringens* iota toxin, respectively (Figure 5 and Figure S5).[35] PA_{63}, C2IIa, and Ib share a high level of amino acid homology and numerous structural and functional similarities, including the ϕ-clamp, essential for the translocase activity of the channels. Like PA_{63}, C2IIa and Ib channels have evolved to translocate the enzymatic components of the related binary toxins into the cytosol. On the contrary, other bacterial toxins, e.g., α-hemolysin of *S. aureus*[36] and epsilon toxin of *C. perfringens*,[37] which act by perforating host cell membranes, are free of the $1/f$-type flickering (Figure S6). The single-channel current noise spectra of other large β-barrel membrane

https://doi.org/10.1021/acs.jpcb.0c10490
J. Phys. Chem. B 2021, 125, 5466−5478

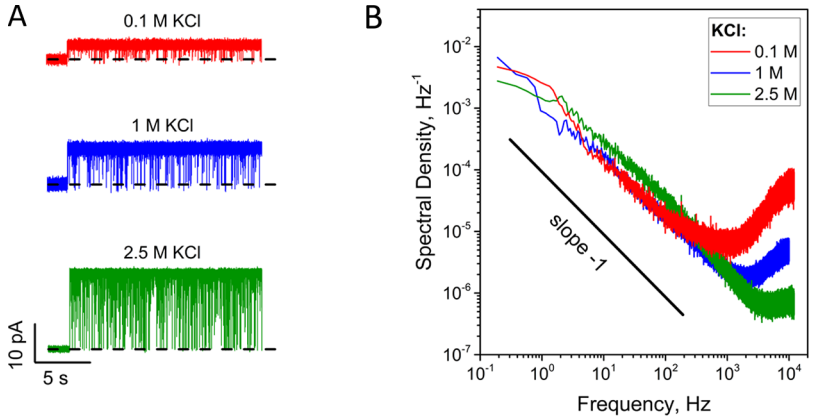

Figure 2. PA_{63} fluctuation dynamics in solutions of different KCl concentrations. (A) Current tracks of a single PA_{63} channel in bathing KCl solutions of different concentrations, 0.1, 1, and 2.5 M. It is seen that the flicker noise appears in all the current tracks. (B) In the $\log_{10}$–$\log_{10}$ scale, the power density spectra for all the current tracks in panel (A) change linearly with frequency at a wide 10−1000 Hz range of frequencies (slope = ∼(−1.0)), which is the typical characteristic of the $1/f$ process. When normalized, dividing by the mean current squared, the power spectral density of $1/f$ noise nearly overlaps at 0.1−100 Hz. The experiments were conducted in KCl solutions buffered at pH 6 (5 mM MES), under 50 mV transmembrane voltage. The current tracks (A) are given at 1 ms resolution.

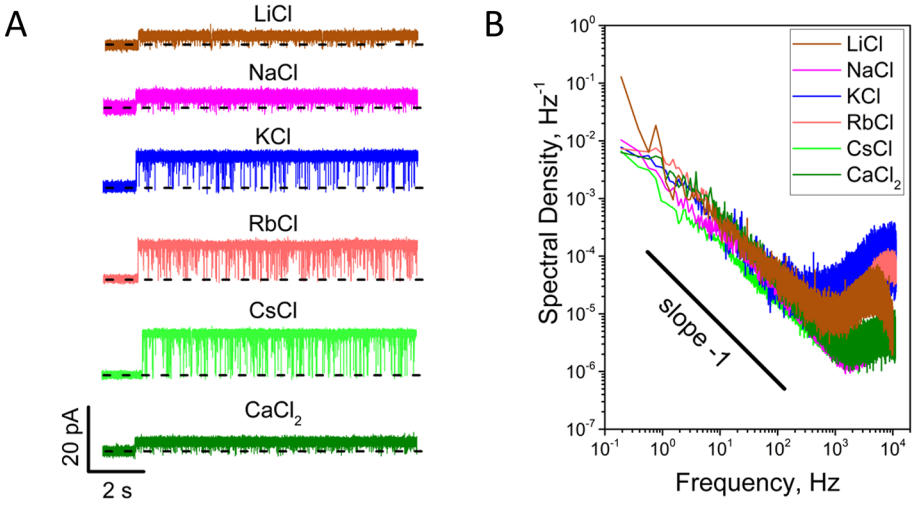

Figure 3. PA_{63}'s $1/f$ noise when reconstituted into model bilayers bathed by different alkaline and alkaline-earth chloride solutions. (A) Current tracks of a single PA_{63} channel in bathing solutions with different cations: LiCl, NaCl, KCl, RbCl, CsCl, and $CaCl_2$. The conductance of PA_{63} is dependent on the nature of the cations of the bathing solution. At the same time, the flicker noise appears in all the current tracks. (B) In the $\log_{10}$–$\log_{10}$ scale, the power density spectra for all the current tracks in panel (A) change linearly with frequency at a wide 10−1000 Hz range of frequencies (slope = ∼(−1.0)), which is the typical characteristic of the $1/f$ process. To account for differences in average conductance in different solutions, the spectral densities were normalized by dividing by average current squared. The experiments were conducted using 1 M solutions of each salt, buffered at pH 6 (5 mM MES), under 50 mV transmembrane voltage. The current tracks (A) are given at 1 ms resolution.

proteins, e.g., OmpF[49] from the outer membrane of *Escherichia coli*[50] and VDAC[51] from the mitochondrial outer membrane, also do not contain the $1/f$ noise component. The only exception that we are aware of is the maltodextrin-specific maltoporin channel of *E. coli* (also known as LamB), where $1/f$ fluctuations were detected in a form of slow (f < 300 Hz), low-amplitude, stepwise open-channel transitions,[21] essentially distinct from the $1/f$ noise in PA_{63}, C2IIa, and Ib channels. The universality and unique characteristics of the flicker noise suggested that it may play a certain role in PA_{63} and other binary toxin channel functions and motivated us to further investigate its mechanism.

$1/f$ Noise Is Generated at the Narrow Hydrophobic ϕ-Clamp Region of PA_{63}. The anthrax toxin channel fluctuation dynamics can be altered by removal of the ϕ-clamp (Figure 6). Thus, the F427A PA_{63} mutant, while showing higher single-channel conductance and several different fluctuation states appearing randomly (e.g., see the high and low noise level state fragments highlighted with the green and red boxes in Figure 6A, respectively), was free of the flickering between the open and closed states detected in the WT PA_{63}. The time hierarchy of the F427A mutant current noise was also different (Figure 6B and Figure S7). The power spectral density of the high-noise fragment is frequency-independent (green spectrum), which is typical for white noise. Even though the power spectral density of the low-noise fragment might resemble the $1/f$ process (red spectrum), it lacks the complete open/closed-channel current transitions (Figure 6A, red box) and is observed only at the low, f < 100 Hz, frequencies. Moreover, the signal power of this noise is 3 orders of magnitude lower than that in WT PA_{63} (blue spectrum). Overall, we can conclude that the fast flickering

https://doi.org/10.1021/acs.jpcb.0c10490
J. Phys. Chem. B 2021, 125, 5466−5478

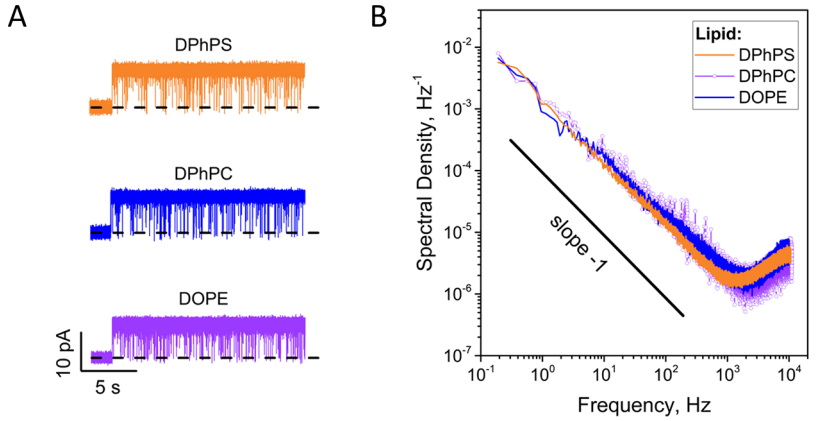

Figure 4. Fluctuation dynamics of a single PA_{63} channel in lipid membranes of different composition. (A) Current tracks (1 ms resolution) of a single PA_{63} channel in negatively charged DPhPS (top), neutral lamellar DPhPC (middle), and nonlamellar DOPE (bottom) membranes. (B) Spectral density analysis of the current fluctuations through a single PA_{63} channel in different lipids shows the characteristic $1/f$ noise behavior. The measurements were conducted in 1 M KCl solutions (5 mM MES), under 100 mV transmembrane voltage at pH 6.

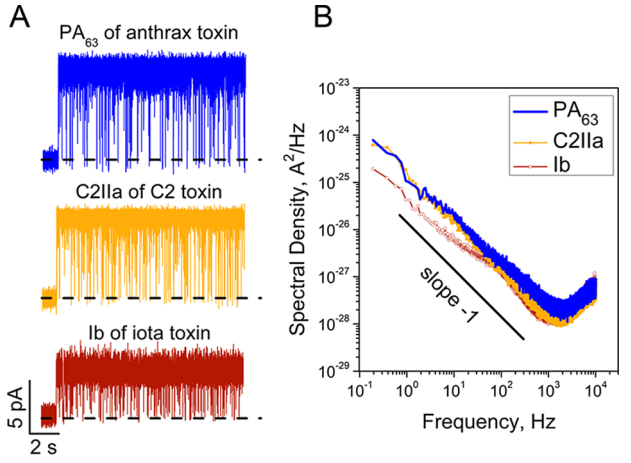

Figure 5. PA_{63}, C2IIa, and Ib single-channel fluctuation dynamics. (A) The single PA_{63}, C2IIa, and Ib channel current tracks show fast flickering between the completely open and closed states, characteristic for the binary bacterial toxin channels. The current tracks are given at 1 ms time resolution. (B) The power spectral density analysis of current recordings, fragments of which are given in panel (A), demonstrates $1/f$ noise behavior in all three channels. At 0.1−1000 Hz frequencies, in the log−log scale, the $1/f$ noise current fluctuations have comparable slopes, which are close to −1. Note that at $f > 30$ Hz, the Ib spectrum (*vinous*) has an additional open-state current noise component. The measurements were performed in 1 M KCl at pH 6.0 (5 mM MES) under 50 mV transmembrane voltage.

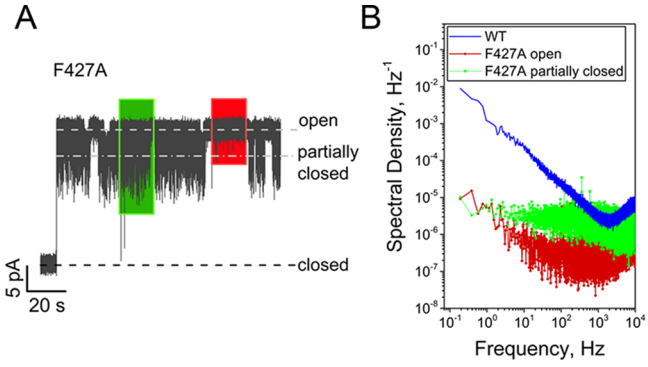

Figure 6. The ϕ-clamp removal disrupts $1/f$ noise behavior. (A) A typical single F427A PA_{63} channel current fluctuation dynamics. Several conductance states were observed; here, the noisiest state is marked with a green box, and the quietest, completely open state, is marked with a red box. Practically no current transients between the completely open and closed states are detected. The currents are given at 1 ms time resolution. (B) The power spectral densities show the difference in the current noise characteristics through WT and F427A PA_{63} mutant channels. The green and red spectra were plotted using the noisiest and quietest current recording fragments marked by the green and red boxes, respectively, in panel (A). The recordings are normalized dividing by the average current squared; the original spectra are provided in Figure S7. The measurements were done in 1 M KCl at pH 6 (5 mM MES) under 50 mV transmembrane voltage.

between the open and closed states observed in WT PA_{63} is absent in F427A PA_{63}. Therefore, it appears that the $1/f$ noise process is generated at the ϕ-clamp region, where the hydrophobic bottleneck of the channel lumen is located. In other words, the $1/f$ noise is likely to occur because of brief small-ion current interruptions at the ϕ-clamp.

We can propose several models to describe the $1/f$ noise mechanism in PA_{63}. The flicker events can be caused by small-scale stochastic movement of the F427 residues, occasionally creating an impermeable physical barrier for the small-ion current. If this is the case, analogous to the PA_{63} voltage gating,[47] we would rather expect this process to be influenced by at least some of the external factors that we tested, namely, applied voltage, electrolyte solution composition, pH, and lipid membrane content. Alternatively, the flicker events can embody the momentary exclusion of water due to the strong hydrophobicity of the ring (the so-called hydrophobic gating[27−29,31,32]), which would reversibly interrupt the passage of water molecules and, therefore, small ions flowing with water through the ϕ-clamp. In this case, the channel is not physically occluded, but the so-called "hydrophobic gate" is formed for water to permeate.[32] A combination of these two mechanisms should also be considered, specifically the movement of F427 residues, coupled with a stochastic wetting and dewetting of the hydrophobic region of the channel,[52] which can cause the $1/f$ closures. To make a distinction between these models, let us turn to the 2.9 Å cryo-EM structure of PA_{63} that shows the ϕ-clamp region being as narrow as 6 Å in diameter.[25] This value is twice as small as the one determined earlier (12 Å) based on tetraalkylammonium ion permeation studies.[53] At the same time, taking into account that the PA_{63} is able to translocate LF and EF with the

https://doi.org/10.1021/acs.jpcb.0c10490
J. Phys. Chem. B 2021, 125, 5466−5478

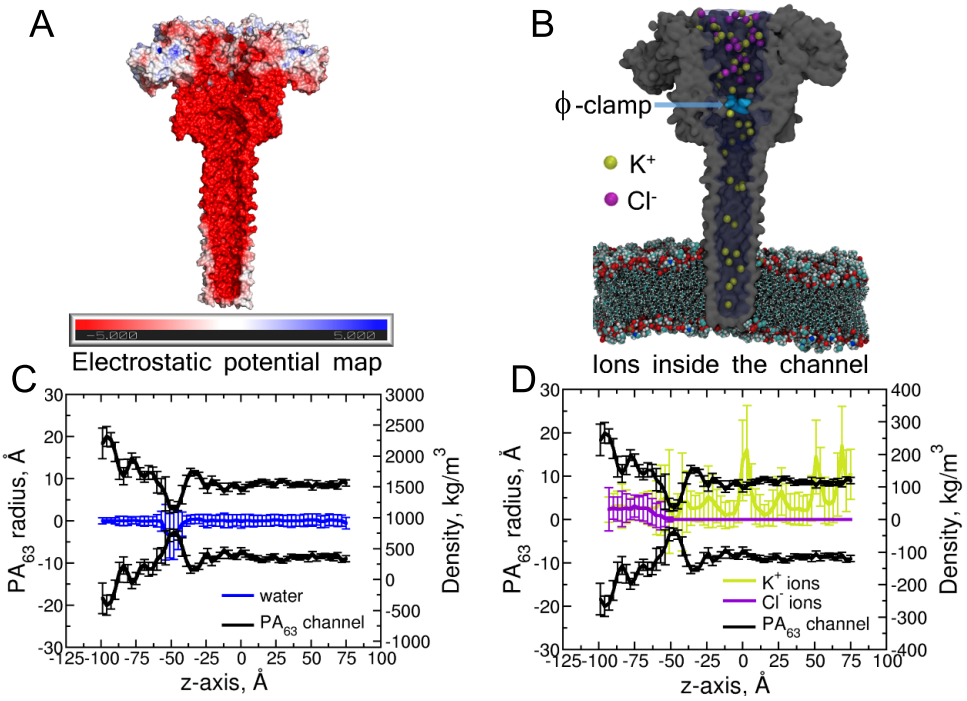

Figure 7. Characterization of the PA_{63} channel using molecular dynamics. (A) The electrostatic potential map of a cross-sectional view of the PA_{63} channel illustrates the highly negatively charged channel interior. (B) A cross-sectional view of ion arrangements inside the PA_{63} in the presence of 1 M KCl. The K^+ and Cl^- ions are shown in yellow and violet, respectively. Only K^+ ions are observed in the region below the ϕ-clamp. (C) Axial variation of the water density and the channel radius. A relatively lower water density (~750 kg/m^3) region around the vicinity of the hydrophobic ϕ-clamp ($z = -50$ Å) is observed. (D) Axial variation of the ion densities. Cl^- is present in -100 Å $< z < -50$ Å and absent in the -50 Å $< z <$ 75 Å region. The distinct peaks seen in the K^+ density profile correspond to the cation binding sites in the channel lumen.

side chains varying in diameter,[54] Jiang et al.[25] proposed that the ϕ-clamp might act as an elastic sealed "O-ring" that changes its size and shape to allow the enzymatic components to translocate effectively. Therefore, it is possible that the cryo-EM has captured the ϕ-clamp in its partially closed, 6 Å configuration, while in the fully open PA_{63} conformation, the channel's bottleneck can be as wide as 12 Å. It was also suggested that the ϕ-clamp can undergo dynamic transitions between the different conformation states when reconstituted in the model bilayers.[48] Note that the concept of "hydrophobic gating" involves water molecules exhibiting liquid−vapor transition within hydrophobic gates of a diameter less than ~14 Å.[32] Therefore, even in the limiting case of the ϕ-clamp being as wide as 12 Å and nondynamic, the hydrophobic gating mechanism of the observed fast flickering is likely.

Characterization of PA_{63} Channel Current by Molecular Dynamics Simulations. We have run molecular dynamics (MD) simulations of the membrane-inserted PA_{63} channel for 1.0 μs in 0.15 and 1 M KCl solutions and computed the root-mean-square-deviation (RMSD) value of PA_{63} with respect to its minimized initial structure to quantify the conformational changes of the protein channel (Table S1, Figure S8). The initial and final simulation snapshots of PA_{63} membrane complexes, which are very stable at both KCl concentrations, are shown in Figure S8A,B, respectively. The RMSD (Figure S8C) increased significantly within the first 2 ns of simulation time, which corresponds to the large conformational changes in the channel structure. Afterward, the profiles increased gradually between 2 to 300 ns of simulation time and reached a plateau of ~3.8 (0.15 M KCl) and ~3.0 Å (1 M KCl). The conformational changes in the N-terminus of protomers are observed due to their unbinding and rebinding with the N-terminus of neighboring protomers in the pore complex. The effect also corresponds to the humps observed at 150−300 ns in the RMSD profile at 0.15 M KCl. To understand the structural changes in the heptameric channel, the secondary structure profiles are analyzed at 0.15 and 1.0 M KCl using the VMD secondary structure analysis tool[55] (Figure S9A). It is seen that the major structural changes in PA_{63} are due to the conformational changes in the secondary structure of α-helices (Figure S9B), which are more significant in the presence of 0.15 M KCl than of 1.0 M KCl. This finding is in good agreement with the RMSD profile trends that we observed. Thus, a distinct property of PA_{63}, known as voltage gating, which is likely to be caused by structural changes, was indeed reported to be enhanced at low KCl solution concentrations.[22,35]

The electrostatic potential map (EPM) calculations of PA_{63} (Figure 7A) demonstrated that the channel lumen is highly electronegative, having a net negative (−49e) charge, which corresponds to conditions where the histidine residues of the PA_{63} channel are nonprotonated. The channel is known to show a strong preference for cations.[56] The cross-sectional view of the K^+/Cl^- ion arrangement inside the PA_{63} is shown in Figure 7B. While both K^+ and Cl^- are present in the wide cap region of the channel (above the ϕ-clamp), only K^+ ions can be detected in the narrow stem region (below the ϕ-clamp). To understand the cation selectivity of the channel, we have computed the channel radius and ion/water density profiles along the channel axis (Figure 7C,D). The channel radius was calculated based on the fractional volume occupied by water inside the channel. We divided PA_{63} into circular slabs of 3 Å width along the axis of the channel (z-axis). The fraction of water molecules to the total number of atoms

https://doi.org/10.1021/acs.jpcb.0c10490
J. Phys. Chem. B 2021, 125, 5466−5478

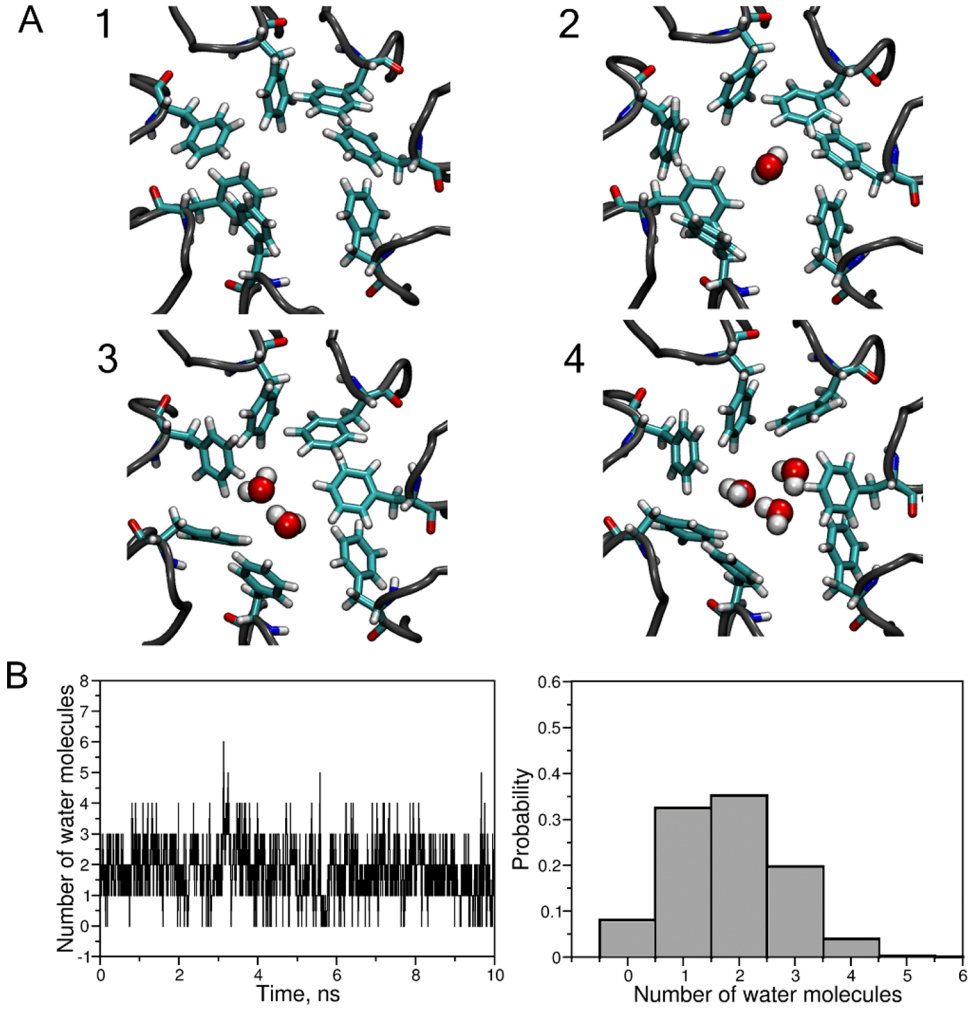

Figure 8. Characterization of water hydration around the ϕ-clamp. (A) The simulation snapshots correspond to different arrangements of water molecules near the ϕ-clamp region (cyan). The O and H atoms of water molecules are shown in VDW representation with red and gray colors, respectively. The snapshot (1) shows no water present, (2) a single water wire formation, (3) a double water wire formation, and (4) a triple water wire formation. (B) The number of water molecules as a function of simulation time (left) and probability distribution of water molecules inside the PA_{63} near the ϕ-clamp region (within $\Delta z = 3.0$ Å from the center of mass of ϕ-clamp) (right) for the last 10 ns of production run. The channel water density at the ϕ-clamp consists of $1 \leq N_w \leq 3$ water molecules most of the time, demonstrating the hydrophobic nature of the ϕ-clamp. The probability of closed state ($N_w = 0$) at the ϕ-clamp region equals to 8%, exceeding the probability observed experimentally.

occupied inside each slab of the channel was computed radially outward from the axis of the slab with a bin width of 0.5 Å. The channel radius (r) was defined as the radial distance from the axis of the channel to the bin where the fraction (the number of water molecules/the total number of atoms) drops below 20%. Earlier, a similar method has been used to calculate the radius profiles of the α-hemolysin and cytolysin A channels.[57,58] The ion/water mass density $\frac{M}{dz2\pi r}$ was computed using the channel radius of each slab along the axis of the channel, where M is the mass of ions/water within slab width dz and r is the channel radius.

The radius profile calculation shows that the PA_{63} channel has a 40 Å extracellular diameter at $z = -100$ Å, and the diameter decreases nonuniformly to a minimum value of ~6 Å at the ϕ-clamp, $z = -48$ Å, region (Figure 7C,D). The channel diameter remains relatively uniform, 20 Å, in the β-barrel region, -25 Å $< z <$ 75 Å. The narrow 6 Å diameter of the channel at the ϕ-clamp can only allow one or two water molecules/ions to translocate at a given time. The decrease in water density (Figure 7C) at the ϕ-clamp reflects the hydrophobic nature of this region, whereas the larger error bars suggest an increase in the flexibility of the aromatic rings of F427 residues. To describe the ϕ-clamp flexibility, the PA_{63} radius was examined as a function of time (Figure S10). The observed significant fluctuations in the channel radius at the ϕ-clamp region are responsible for the large error bars in the water density inside the channel. The axial ion density profiles (Figure 7D) reveal the presence of K^+ ions both above and below the ϕ-clamp. We have also detected distinct peaks in the K^+ density profile (Figure 7D) at z = 2, 52, 72, and −27 Å, visualized as the locations of K^+ crowding in the channel lumen (Figure 7B). We suggest that these peaks may correspond to the cation binding sites inside the PA_{63} channel, provided by negatively charged glutamic acid and aspartic acid amino acids, namely, E170, E593, E1016, E1439, E1862, E2285, and E2708 at z = 2 Å, E129, E552, E975, E1398, E1821, E2244, and E2667 at z = 52 Å, E135, E558, E981, E1404, E1827, E2250, and E2673 at z = 72 Å, and D162, D593, D1016, D1439, D1862, D2285, and D2708 at $z = -27$ Å (Figure 7D).

https://doi.org/10.1021/acs.jpcb.0c10490
J. Phys. Chem. B 2021, 125, 5466−5478

Structure of Water Hydration Around the ϕ-Clamp. To describe the local hydration conditions at the ϕ-clamp, we have generated four different hydration simulation snapshots near the region (Figure 8A). The ϕ-clamp hydration is less dense than the bulk regions. First, there are several instances when water is absent in the ϕ-clamp region (Figure 8A (1)). Second, water at the ϕ-clamp region can form single or multiwire arrangements (Figure 8A (2−4)). This type of water arrangement, which corresponds to the lower water density values seen at z = 48 Å (Figure 7C), can be explained by the ϕ-clamp region hydrophobicity. To quantify the observed exclusion of water, we calculated the number of water molecules at the ϕ-clamp as a function of simulation time (Figure 8B, left panel) and determined the corresponding water residing probabilities (Figure 8B, right panel). It is seen that the number of water molecules (N_w) in the ϕ-clamp fluctuates as a function of simulation time from a dewetted to fully hydrated state, $0 \leq N_w \leq 7$ (Figure 8B, left panel). Importantly, the ϕ-clamp typically contains only 1−3 water molecules ($1 \leq N_w \leq 3$) concurrently (Figure 8B, right panel), with a probability of being in the closed, dewetted ($N_w = 0$), state being equal to 8%.

PA_{63} Ion Conductance. The nature of the ion current profile is an important characteristic of protein channels. To measure the ionic current, we applied an external electric field, E = 0.05 and E = 0.5 V/nm, along the positive z-direction. During the MD simulations under the applied electric field, the lipid membrane was constrained to its initial configuration using a harmonic constraint. Constraints were applied only in the z-direction, and lipids were allowed to move in the x−y plane. The instantaneous ionic current, $I(t)$, is measured across the transmembrane part of the protein channel using the following equation

$$I(t) = \frac{1}{\delta t L_z} \sum_{i=1}^{N} q_i[z_i(t + \delta t) - z_i(t)]$$

where z_i and q_i are the z coordinate and atomic charge of the ith atom, respectively, N is the total number of ions present in the system, and L_z is the membrane thickness (5 nm). Coordinates of the ions were recorded every 1.5 ps to compute the ionic current. The value of δt is 1.5 ps; however, we have verified that different values of δt produce very similar current profiles. We have run 35 ns-long MD simulations for ionic current measurements. The ion current profiles of K^+ and Cl^- as a function of simulation time, computed with 0.05 and 0.5 V/nm electric field strengths for 0.15 and 1.0 M KCl concentrations, are shown in Figure S11A−D. In all four cases, the Cl^- current reduces to zero after reaching a steady state. As described above, the effect is due to the strong electrostatic repulsion between negatively charged Cl^- ions and negatively charged channel lumen residues located below the ϕ-clamp, z > −48 Å, region (see also Figure 7A,B,D). The K^+ currents under E = 0.05 V/nm are almost continuous (Figure S11A,C) due to the fact that K^+ ions have lower mobilities and take more time to translocate through the channel under a low electric field. In addition, the K^+ ion current oscillates around the mean value, and the larger negative amplitude current is observed for a lower field strength of E = 0.05 V/nm due to the movement of the K^+ ions in the opposite direction of the applied field as a result of thermal fluctuations. In contrast, lower negative amplitude currents are observed under a high field strength of E = 0.5 V/nm as the K^+ ion motion is dominated by the applied electric field, which is much stronger than the thermal fluctuation. Hence, the average ion current inside the channel is lower at E = 0.05 V/nm than at the high electric field case (E = 0.5 V/nm). In contrast to E = 0.05 V/nm, K^+ ion currents become discontinuous under a higher electric field, E = 0.5 V/nm, (Figure S11B,D), both in 0.15 and 1 M KCl, and the average ion current through PA_{63} is larger than that in the 0.05 V/nm case. To further investigate PA_{63} channel conductivity, we computed the average ionic current inside the channel with different applied voltages (Figure S12). The current turned out to be directly proportional to the applied voltage. The discontinuity/flickering of current observed in K^+ current profiles under the higher electric field is due to the gating of K^+ current at the ϕ-clamp region of the channel.

Free Energy of Water and Ions. To understand the free energy barrier for water and K^+/Cl^- ions across the ϕ-clamp region of the channel, we calculated the potential of mean force (PMF) as a function of their distance from the ϕ-clamp (at z = 0 Å) along the z-axis (Figure S11E). The PMF profile of water indicates that the free energy barrier for the water molecules to cross the ϕ-clamp region is small; it can be overcome by their thermal fluctuations, and in general, water molecule translocation across the ϕ-clamp is energetically favorable (1.8 kcal/mol). The energy barriers for ions to translocate across the ϕ-clamp (z > 0) are much higher, 4.0 and 6.5 kcal/mol for K^+ and Cl^-, respectively, in the absence of the electric field. Therefore, only the water molecules can permeate through the ϕ-clamp region at thermal equilibrium. Under an external electric field, there is an additional force acting on K^+ ions in the direction of the field (z > 0), while a similar force acts in the opposite direction (z < 0) for Cl^-. This additional applied force, acting on the K^+ ions, is sufficient to overcome the potential barrier present at the ϕ-clamp region allowing for the K^+ ion permeation across PA_{63}. However, in the case of Cl^- ions, it enhances the barrier height at the ϕ-clamp region preventing any Cl^- current. The PMF profile of the K^+ ion in the presence of an electric field indicates that the potential barrier of the K^+ ion at the ϕ-clamp decreases, and the translocation of K^+ ions across the region becomes energetically favorable by ∼3 kcal/mol. In contrast, the potential barrier for Cl^- ions at the ϕ-clamp increases from 6.5 to 10.0 kcal/mol, which results in the zero Cl^- ion current profiles (Figures 4 and 7D, Figure S11A−D).

On Hydrophobic Gating and 1/f Noise of PA_{63}. The 1/f noise in the PA_{63} channel appears to be generated at the ϕ-clamp region. In this study, we hypothesized that the ϕ-clamp forms a narrow hydrophobic gate, specifically an energetic barrier for water and, concurrently, ion permeation.[59] If this is the case, the flicker noise can represent the wetting/dewetting process of the ϕ-clamp gate, which leads to the channel stochastically switching from a permeable to impermeable state without being physically occluded (the so-called liquid−vapor transitions).[32] The stochastic dewetting of the region creates an energetic barrier for ion permeation. We validated this hypothesis by performing all-atom molecular dynamics simulations, which can effectively capture the essentials of water and ion permeation through membrane channels of known structures. As expected, the MD simulations revealed PA_{63} being largely selective for K^+ due to the presence of a large number of negatively charged residues in the channel lumen and the additional energetic barrier for Cl^- permeation created by the ϕ-clamp (Figure 7A,B,D). More importantly,

https://doi.org/10.1021/acs.jpcb.0c10490
J. Phys. Chem. B 2021, 125, 5466−5478

analysis of the averaged water density in the PA_{63} lumen showed that there is a 24% decrease in water density at the ϕ-clamp region compared to the cap and stem parts of the channel (Figure 7C). Direct visualization of the local ϕ-clamp hydration arrangements in the form of four simulation snapshots (Figure 8A) revealed instances when water is completely absent from the ϕ-clamp and when one or two water molecules are present. The K^+ current profiles, examined as a function of simulation time under an electric field of 0.5 V/nm, had a discontinuous pattern (Figure S11B,D), showing that the stochastic channel dewetting events result in ion current interruptions.

While the hydrophobic gating phenomenon was first predicted computationally,[26] several subsequent experimental studies have employed the concept of hydrophobic dewetting to explain the nature of the nonconductive state in a number of biological ion channels.[52,60−66] Questions remain over comparability between the dewetting events on the nanosecond timescale detected computationally with millisecond and microsecond timescales obtained from the single-channel noise analysis (see related discussion in ref 32). Despite these well-appreciated differences in timescales, the all-atom simulations provide several molecular insights into both the wetting-dewetting phenomenon and the ion transport characteristics across the ϕ-clamp. While it will not solve the general timescale comparability problem, we want to emphasize that the current noise spectral analysis mostly allows us to capture the longest (<2000 Hz or >0.5 μs) flicker events, while the multiple faster events are either not resolved (Figure S13) due to the bilayer setup limitations (15 μs) or suppressed by the high-frequency background noise. We also observed some discrepancies between the nonconductive-state probabilities; its value calculated using MD simulations (p^{MD}_{dewet} = 0.08 ± 0.01) exceeded what was obtained from single-channel measurements (p^{SCh}_{dewet} = 0.0070 ± 0.0005). To explain this difference, let us get back to the cryo-EM structure of the PA_{63} channel,[25] which shows the ϕ-clamp being 6 Å in diameter. Interestingly, before the structure became available, the diameter of the narrowest region of the channel was believed to be ≈12 Å because ligands of this size were able to permeate through the channel.[53] It remains to be seen if the open PA_{63} conformation that we investigated in the model bilayers, which allows molecules up to 12 Å to penetrate, is different from the structure reported by the cryo-EM structure used in our MD simulations study. Thus, it was suggested that in order to effectively translocate LF and EF with the side chains varying in diameter, the ϕ-clamp might act as an elastic sealed "O-ring" that changes its size and shape.[25] If that is the case, the cryo-EM might have captured the ϕ-clamp in its partially closed, 6 Å configuration, while in the fully open PA_{63} conformation investigated in the bilayers, the channel's bottleneck can be as wide as 12 Å. The ϕ-clamp can stochastically switch between varieties of different diameter conformations, each having a different effect on the liquid−vapor probability transition.[32] The dynamic hydrophobic seal model of protein translocation was also suggested in the recent cryo-EM study that captured a snapshot of the PA_{63} channel translocating LF_N.[67] The authors report detecting motion of the ϕ-clamp residues (concerted or individual), which may move up and down to accommodate different side chains. In addition, the idea about the dynamic behavior of the ϕ-clamp was directly supported in a study when F427 was site-specifically labeled with *p*-fluorophenylalanine and investigated using ^{19}F NMR.[68] We suggest that this is the reason why, instead of being described by the two-state Markov process (wetted and dewetted states), the process has a characteristic $1/f$-like behavior. The ϕ-clamp dynamics can also partially explain the observed difference between the experimental and computational timescales of the events. The performed MD simulations calculated the hydrophobic dewetting event timescales, while in the planar lipid bilayer measurements, we likely detect the hydrophobic gating events coupled with the ϕ-clamp dynamic movements. In a certain sense, we combine two fundamentally different $1/f$ noise models in ion channels and nanopores.[69] The first model implies that the flicker noise in nanopores can be caused by the small-scale conformational fluctuations of the open channel[21] or channel opening and closing.[23] The second model suggests that the origin of $1/f$ noise cannot be attributed to fluctuations of the channel geometry alone; instead, local fluctuations of the liquid conductivity should also be taken into account.[70]

CONCLUSIONS

The flicker noise is detected as voltage-independent $1/f$ fluctuations between the completely open and closed states of the channel-forming components of the binary anthrax, C2, and iota toxins generated at the ϕ-clamp region. We hypothesized that because the process is likely to represent hydrophobic gating and because it concurs with the channels' translocase activity, the stochastic wetting/dewetting at the ϕ-clamp plays a central role in the toxin's intracellular uptake. However, the role of hydrophobic gating and its possible contribution to the protein transport process remain an open question. Traditionally, hydrophobic gating is used to explain the regulation of the flow of small ions, by changes in the channel's hydrophobic region hydration. In this context, we can suggest that the hydrophobic gating in PA_{63}, C2IIa, and Ib exists to avert leakage of protons across the endosomal membranes. Maintenance of the transmembrane endosomal pH gradient is critical for the binary toxin uptake, yet the highly cation-selective toxin channels, if not regulated, can impair the gradient, especially at high toxin concentrations. The tuned ionic composition of endosomes[71] is also vital for their function. One can argue that the closed-state probability detected in planar bilayers is too low to effectively prevent the proton and ion leak. However, the probability of finding the channel in the closed state is increased by the presence of PA_{63}-bound LF.[72] Moreover, in the crowded in vivo environment, there are other factors that can shift the wetted/dewetted-state equilibrium. Therefore, the process that appears subtle in vitro may play an important regulatory role in physiological conditions. Similarly, it was suggested that the role of hydrophobic gating in the SecY protein translocation pore is to prevent leakage of water and ions in the absence of a translocating peptide.[73] Alternatively, if we exceed the limits of the traditional hydrophobic gating functional interpretation, we can suggest that the stochastic wetting/dewetting process at the ϕ-clamp may be vital for the LF and EF translocation. At first sight, this interpretation may appear paradoxical because water exclusion is expected to prevent transport of any substance, not only small ions through the ϕ-clamp. However, if we ponder over earlier suggestions about the importance of the F427 ring for LF and EF binding and translocation,[74,75] the idea falls into place. To be effective, the F427 ring might interact with both the substrate cationic side-chains (via cation−π interactions) and hydrophobic sequences (via π−π

https://doi.org/10.1021/acs.jpcb.0c10490
J. Phys. Chem. B 2021, 125, 5466−5478

interactions or hydrophobic contacts),[33] possibly adjusting its own size to accommodate their different dimensions.[25] To discriminate between different substrate sequence segments, the toxin could have been evolved not only to stochastically alter the size of the channel constriction but also the region hydration. Thus, the dewetting transition is known to induce long-range attraction between different hydrophobic objects.[76] Finally, a combination of the suggested mechanisms is also possible. In particular, the importance of the ϕ-clamp acting as a hydrophobic seal, maintaining the proton gradient, which serves as a driving force for the enzymatic toxin component translocation, has been also investigated.[77] If so, the hydrophobic gating, manifested by the $1/f$ noise that we discuss here, could be the mechanism to uphold the gradient.

EXPERIMENTAL SECTION

Chemicals. Recombinant *Bacillus anthracis* WT PA_{83}, F427A PA_{83} mutant, and (D512K + K245G-R252N) bicomponent octameric variant of PA were produced as described in refs 35, 45, 78. PA_{63} was prepared from PA_{83} using furin[79] or purchased from List Biological Laboratories, Inc. (Campbell, CA, USA) in the purified form. The following chemical reagents were used: KCl, NaCl, LiCl, CsCl, RbCl, $CaCl_2$, MES, KOH, NaOH, LiOH, CsOH, RbOH, $Ca(OH)_2$, HCl (Sigma-Aldrich, St. Louis, MO, USA), "purum" hexadecane (Fluka, Buchs, Switzerland), pentane (Burdick and Jackson, Muskegon, MI), and agarose (Bethesda Research Laboratory, Gaithersburg, MD). 1,2-Diphytanoyl-*sn*-glycero-3-phosphocholine (DPhPC), 1,2-diphytanoyl-*sn*-glycero-3-phospho-L-serine (DPhPS), and 1,2-dioleoyl-*sn*-glycero-3-phosphoethanolamine (DOPE) were purchased from Avanti Polar Lipids, Inc., Alabaster, AL, USA (all in chloroform). Milli-Q water (EMD Millipore, Billerica, MA, USA) was used to prepare solutions.

Ion-Channel Reconstitution. "Solvent-free" planar lipid bilayer membranes were formed following the lipid monolayer opposition technique.[80] The lipid bilayer cell was custom-made using a two-compartment (*cis* and *trans*) Teflon chamber separated by a 15 μm-thick Teflon partition with ~60 μm diameter aperture for membrane formation. A 1.5 mL quantity of (0.01−2) M KCl solutions buffered at pH 4.5−7.5 (5 mM MES) was added to both *cis* and *trans* sides of the chamber symmetrically. The membranes were made by *cis* and *trans* addition of 10−20 μL of 5 mg/mL stock lipid solution (predried from chloroform using nitrogen gas). To secure membrane formation, ~2−3 μL of 1% (v/v) hexadecane/pentane solution was added directly on the film and then air-dried for ~10 min. Single channels were formed by adding 0.2−1 μL of 1 μg/mL solution of WT PA_{63} or 2−4 μL of 0.5 mg/mL solution of F427A PA_{63} or (D512K + K245G-R252N) PA_{63} to 1.5 mL of the aqueous phase in the *cis* half of the chamber after bilayer formation. Under this protocol, the channel insertion was always directional as judged by an asymmetry in PA_{63} voltage gating toward the applied voltage.[56]

The electrical potential difference across the membrane was applied, and the current signal was recorded with a pair of Ag-AgCl electrodes in 2 M KCl, 1.5% agarose bridges assembled within standard 200 μL pipette tips. The measurements were taken at room temperature, (23 ± 0.5) °C. The current was amplified by an Axopatch 200B amplifier (Molecular Devices, LLC, San Jose, CA, USA) in the voltage clamp mode (whole cell β = 0.1 for multichannel and β = 1 for single-channel measurements) with a CV-203BU headstage. Data were digitized with Digidata 1440A, while the output signal was filtered by a low-pass 8-pole Butterworth filter (model 900, Frequency Devices Inc., Ottawa, IL, USA) at 15 kHz and directly saved into the computer memory with a sampling frequency of 50 kHz (for single-channel measurements) and 50 Hz (for multichannel measurements). The membrane chamber and headstage were isolated from external noise sources with a double μ metal screen (custom ordered from Amuneal Manufacturing Corp., Philadelphia, PA, USA). Current fluctuation analysis was performed using ClampFit 10.7 software (Molecular Devices, LLC, CA, San Jose, USA), OriginPro 8.5 (OriginLab, Northampton, MA, USA) software, and with software developed in-house. All experiments were repeated at least three times using fresh planar lipid membrane preparations. The ion current noise spectral density analysis was performed as described by Bendat and Piersol.[41] Because of the high reproducibility of the PA_{63} current noise response, randomly chosen results from representative experiments are shown.

Simulation Methodology. The structure and dynamics of the anthrax toxin protective antigen protein channel embedded in the lipid membrane were investigated using molecular dynamics simulations. The 1-palmitoyl-2-oleoyl-*sn*-glycero-3-phosphocholine (POPC) lipid bilayer was used to model the lipid membrane. A lipid bilayer of cross section 165 Å × 165 Å having 400 lipids in each leaflet was constructed using the CHARMM-GUI membrane builder.[81] The atomic coordinates of the PA_{63} protein channel (PDB ID 3J9C)[25] were downloaded from the Protein Data Bank. It is worth mentioning here that earlier simulations involving the PA_{63} protein channel[47,82] used a computational model structure (PDB ID 1V36) instead of the more accurate cryo-EM structure used in this work. We first created a channel of 10 Å radius in the middle of the lipid bilayer to embed the protein channel in the lipid bilayer. Subsequently, the PA_{63} complex was placed inside the membrane channel such that the channel axis is aligned along the membrane normal (z-axis) (Figure S8A) using VMD.[55] The initial built protein channel embedded lipid-bilayer structure was solvated using TIP3P water with a 15 Å water layer from either ends of the PA_{63} channel along its z-axis. The solvated system was neutralized by adding an appropriate number of K^+ ions to compensate the negative charges of the PA_{63} channel. We have also added extra K^+ and Cl^- ions to achieve the two different (0.15 and 1 M) salt concentrations using the leap module in AmberTools.[83] Periodic boundary conditions (PBC) were employed in all three directions of the simulation box.

All-atom molecular dynamics simulations were performed using the PMEMD module of the AMBER software package.[84] Lipid14 force field (FF)[85] parameters were used to describe the bonded and nonbonded interactions involving the lipid molecules, while the AMBER12SB FF[86] was used to model interaction involving the protein channel. The solvated protein channel-lipid bilayer system was subjected to 1000 steps of the steepest descent energy minimization followed by 2000 steps of conjugate gradient minimization to remove bad contacts between the solute and solvent. During minimization, the solute atoms were fixed to their initial configuration using the position restraints with a force constant of 500 kcal/(mol Å^2). This step was followed by an additional 5000 steps of conjugate gradient minimization by gradually decreasing the position restraints to zero. Subsequently, the energy-minimized structure was gradually heated up from 0 to 300 K. The heated

https://doi.org/10.1021/acs.jpcb.0c10490
J. Phys. Chem. B 2021, 125, 5466−5478

system was then subjected to a 1 μs MD production run in the constant temperature and pressure (NPT) ensemble. A 12 Å cutoff was used to compute the nonbonding interactions for the Lennard-Jones (L-J) potential and short-range part of the electrostatic potentials. The particle mesh Ewald sum (PME) method[87] was used to compute the long-range part of electrostatic potential. All bonds involving hydrogens were constrained using the SHAKE algorithm[88] to achieve the 2 fs time step integration during the MD simulations. The same MD protocol has been used in our previous studies to produce very stable trajectories for various complex systems.[58,89−96]

Umbrella Sampling and Weighted Histogram Analysis Method. Umbrella sampling[97,98] followed by the weighted histogram analysis method[99] (WHAM) is a well-known method routinely used to compute the potential of mean force (PMF) along a given reaction coordinate (ξ). Here, we have computed the PMF of the K^+/Cl^- ions and water molecules as a function of their distances from the ϕ-clamp of PA_{63} along the channel axis (z-axis) using umbrella sampling. The reaction coordinate (ξ) was defined as the distance between the position of ion/water molecules and the center of mass of the ϕ-clamp along the z-direction. We have sampled the reaction coordinate starting from −21 to 21 Å using a force constant of 4.0 kcal/(mol A^2) with a 1.0 Å bin width. Each bin was sampled for 5 ns, and the last 2 ns trajectory was used to obtain the PMF profiles of ions/water molecules.

■ ASSOCIATED CONTENT

Supporting Information

The Supporting Information is available free of charge at https://pubs.acs.org/doi/10.1021/acs.jpcb.0c10490.

Anthrax toxin channel current fluctuation dynamics (three different modes of PA_{63} current fluctuations) (Figure S1), PA_{63} fluctuation dynamics in KCl solutions of different pH (Figure S2), fluctuation dynamics of a single PA_{63} channel in type 1 and type 2, maximum and main state insertion (Figure S3), fluctuation dynamics of a single heptameric WT and octameric (D512K + K245G-R252N) PA_{63} channels (Figure S4), PA_{63}, C2IIa, and Ib single-channel fluctuation dynamics (normalized spectra) (Figure S5), epsilon toxin and α-hemolysin single-channel current recording and spectral analysis (Figure S6), the ϕ-clamp removal disrupts $1/f$ noise behavior (original spectra) (Figure S7), initial and final configurations of the PA_{63} channel embedded in a POPC lipid bilayer and RMSD profiles in 1 and 0.15 M KCl (Figure S8), secondary structure analysis of the PA_{63} channel (Figure S9), PA_{63} radius at the ϕ-clamp region of the channel (Figure S10), the K^+ and Cl^- currents across the PA_{63} channel calculated under the external electric field (Figure S11), characterization of the PA_{63} channel using molecular dynamics (Figure S12), and high-resolution (15 μs) current track of a single PA_{63} channel (Figure S13) (PDF)

■ AUTHOR INFORMATION

Corresponding Author

Ekaterina M. Nestorovich − *Department of Biology, The Catholic University of America, Washington, D.C. 20064, United States;* orcid.org/0000-0001-8777-9800; Phone: 202-319-6723; Email: Nestorovich@cua.edu; Fax: 202-319-5271

Authors

Goli Yamini − *Department of Biology, The Catholic University of America, Washington, D.C. 20064, United States*

Subbarao Kanchi − *Department of Chemical Engineering and Centre for Condensed Matter Theory, Department of Physics, Indian Institute of Science, Bengaluru 560012, India;* orcid.org/0000-0001-9147-0101

Nnanya Kalu − *Department of Biology, The Catholic University of America, Washington, D.C. 20064, United States*

Sanaz Momben Abolfath − *Department of Biology, The Catholic University of America, Washington, D.C. 20064, United States*

Stephen H. Leppla − *Laboratory of Parasitic Diseases, National Institute of Allergy and Infectious Diseases, National Institutes of Health, Bethesda, Maryland 20892, United States*

K. Ganapathy Ayappa − *Department of Chemical Engineering, Indian Institute of Science, Bengaluru 560012, India;* orcid.org/0000-0001-7599-794X

Prabal K. Maiti − *Centre for Condensed Matter Theory, Department of Physics, Indian Institute of Science, Bengaluru 560012, India;* orcid.org/0000-0002-9956-1136

Complete contact information is available at: https://pubs.acs.org/10.1021/acs.jpcb.0c10490

Author Contributions

E.M.N. conceived and supervised the study. G.Y., S.K., K.G.A., P.K.M., and E.M.N. designed the experiments. G.Y., N.K., S.M.A., and E.M.N. performed the experiments. S.K. performed the simulations, and G.Y., S.K., K.G.A., P.K.M., and E.M.N. analyzed and interpreted the data and wrote the manuscript. S.H.L. provided the reagents. G.Y., S.K., N.K., S.M.A., S.H.L., K.G.A., P.K.M., and E.M.N. participated in data discussion and made manuscript revisions.

Notes

The authors declare no competing financial interest.

■ ACKNOWLEDGMENTS

We are thankful to Dr. Holger Barth, Ulm University, Ulm, Germany, for providing C2IIa and to Dr. Michel Popoff, Institut Pasteur, Paris, France, for providing Ib. The project was financially supported by NIAID of the NIH under award number 1R15AI099897-01A1 (to E.M.N.). We thank DST, India, for financial support and Supercomputer Education and Research Center (SERC), IISc for proving the computational facility. G.Y. was supported by the American Dissertation Fellowship from AAUW. S.K. thanks UGC (University Grants Commission, India) for a research fellowship. This research was supported in part by the Intramural Program of the National Institute of Allergy and Infectious Diseases, NIH (S.H.L.).

■ REFERENCES

(1) Tsimring, L. S. Noise in biology. *Rep. Prog. Phys.* **2014**, *77*, No. 026601.

(2) Sejdić, E.; Lipsitz, L. A. Necessity of noise in physiology and medicine. *Comput. Methods Prog. Biomed.* **2013**, *111*, 459−470.

(3) Cohen, L. The history of noise [on the 100th anniversary of its birth]. *IEEE Signal Process. Mag.* **2005**, *22*, 20−45.

(4) Bezrukov, S. M.; Vodyanoy, I.; Parsegian, V. A. Counting polymers moving through a single ion channel. *Nature* **1994**, *370*, 279−281.
(5) Kasianowicz, J. J.; Brandin, E.; Branton, D.; Deamer, D. W. Characterization of individual polynucleotide molecules using a membrane channel. *Proc. Natl. Acad. Sci. U. S. A.* **1996**, *93*, 13770−13773.
(6) Jain, M.; Olsen, H. E.; Paten, B.; Akeson, M. The Oxford Nanopore MinION: delivery of nanopore sequencing to the genomics community. *Genome Biol.* **2016**, *17*, 239.
(7) Parsegian, V. A.; Bezrukov, S. M.; Vodyanoy, I. Watching small molecules move: interrogating ionic channels using neutral solutes. *Biosci. Rep.* **1995**, *15*, 503−514.
(8) White, J. A.; Rubinstein, J. T.; Kay, A. R. Channel noise in neurons. *Trends Neurosci.* **2000**, *23*, 131−137.
(9) O'Donnell, C.; van Rossum, M. C. W. Systematic analysis of the contributions of stochastic voltage gated channels to neuronal noise. *Front. Comput. Neurosci.* **2014**, *8*, 105.
(10) Hille, B. *Ion channels of excitable membranes*; Siunderland: Siunderland, MA, 2001.
(11) Derksen, H. E.; Verveen, A. A. Fluctuations of resting neural membrane potential. *Science* **1966**, *151*, 1388−1389.
(12) Weissman, M. B. A mechanism for 1/f noise in diffusing membrane channels. *Biophys. J.* **1978**, *21*, 87−91.
(13) Sauvé, R.; Szabo, G. Interpretation of 1/f fluctuations in ion conducting membranes. *J. Theor. Biol.* **1985**, *113*, 501−516.
(14) Fuliński, A.; Grzywna, Z.; Mellor, I.; Siwy, Z.; Usherwood, P. N. R. Non-Markovian character of ionic current fluctuations in membrane channels. *Phys. Rev. E* **1998**, *58*, 919−924.
(15) Goychuk, I.; Hänggi, P. Anomalous escape governed by thermal 1/f noise. *Phys. Rev. Lett.* **2007**, *99*, 200601.
(16) Banerjee, J.; Verma, M. K.; Manna, S.; Ghosh, S. Self-organised criticality and 1/f noise in single-channel current of voltage-dependent anion channel. *Europhys. Lett.* **2006**, *73*, 457−463.
(17) Bezrukov, S. M.; Vodyanoy, I., Noise in Biological Membranes and Relevant Ionic Systems. In *Biomembrane Electrochemistry*; American Chemical Society, 1994, Vol. *235*, pp. 375−399, DOI: 10.1021/ba-1994-0235.ch017.
(18) Wohnsland, F.; Benz, R. 1/f-Noise of open bacterial porin channels. *J. Membr. Biol.* **1997**, *158*, 77−85.
(19) Andersen, C.; Cseh, R.; Schülein, K.; Benz, R. Study of sugar binding to the sucrose-specific ScrY channel of enteric bacteria using current noise analysis. *J. Membr. Biol.* **1998**, *164*, 263−274.
(20) Orlik, F.; Schiffler, B.; Benz, R. Anthrax toxin protective antigen: inhibition of channel function by chloroquine and related compounds and study of binding kinetics using the current noise analysis. *Biophys. J.* **2005**, *88*, 1715−1724.
(21) Bezrukov, S. M.; Winterhalter, M. Examining noise sources at the single-molecule level: 1/f noise of an open maltoporin channel. *Phys. Rev. Lett.* **2000**, *85*, 202−205.
(22) Nestorovich, E. M.; Karginov, V. A.; Berezhkovskii, A. M.; Bezrukov, S. M. Blockage of anthrax PA_{63} pore by a multicharged high-affinity toxin inhibitor. *Biophys. J.* **2010**, *99*, 134−143.
(23) Siwy, Z.; Fuliński, A. Origin of $1/f^{\alpha}$ noise in membrane channel currents. *Phys. Rev. Lett.* **2002**, *89*, 158101.
(24) Heerema, S. J.; Schneider, G. F.; Rozemuller, M.; Vicarelli, L.; Zandbergen, H. W.; Dekker, C. 1/f noise in graphene nanopores. *Nanotechnology* **2015**, *26*, No. 074001.
(25) Jiang, J.; Pentelute, B. L.; Collier, R. J.; Zhou, Z. H. Atomic structure of anthrax protective antigen pore elucidates toxin translocation. *Nature* **2015**, *521*, 545−549.
(26) Beckstein, O.; Biggin, P. C.; Sansom, M. S. P. A Hydrophobic Gating Mechanism for Nanopores. *J. Phys. Chem. B* **2001**, *105*, 12902−12905.
(27) Hummer, G.; Rasaiah, J. C.; Noworyta, J. P. Water conduction through the hydrophobic channel of a carbon nanotube. *Nature* **2001**, *414*, 188−190.
(28) Beckstein, O.; Sansom, M. S. P. Liquid-vapor oscillations of water in hydrophobic nanopores. *Proc. Natl. Acad. Sci. U. S. A.* **2003**, *100*, 7063−7068.
(29) Anishkin, A.; Sukharev, S. Water dynamics and dewetting transitions in the small mechanosensitive channel MscS. *Biophys. J.* **2004**, *86*, 2883−2895.
(30) Beckstein, O.; Tai, K.; Sansom, M. S. P. Not ions alone: barriers to ion permeation in nanopores and channels. *J. Am. Chem. Soc.* **2004**, *126*, 14694−14695.
(31) Rasaiah, J. C.; Garde, S.; Hummer, G. Water in nonpolar confinement: from nanotubes to proteins and beyond. *Annu. Rev. Phys. Chem.* **2008**, *59*, 713−740.
(32) Aryal, P.; Sansom, M. S. P.; Tucker, S. J. Hydrophobic gating in ion channels. *J. Mol. Biol.* **2015**, *427*, 121−130.
(33) Krantz, B. A.; Melnyk, R. A.; Zhang, S.; Juris, S. J.; Lacy, D. B.; Wu, Z.; Finkelstein, A.; Collier, R. J. A phenylalanine clamp catalyzes protein translocation through the anthrax toxin pore. *Science* **2005**, *309*, 777−781.
(34) Bachmeyer, C.; Orlik, F.; Barth, H.; Aktories, K.; Benz, R. Mechanism of C2-toxin inhibition by fluphenazine and related compounds: investigation of their binding kinetics to the C2II-channel using the current noise analysis. *J. Mol. Biol.* **2003**, *333*, 527−540.
(35) Bezrukov, S. M.; Liu, X.; Karginov, V. A.; Wein, A. N.; Leppla, S. H.; Popoff, M. R.; Barth, H.; Nestorovich, E. M. Interactions of High-Affinity Cationic Blockers with the Translocation Pores of B. anthracis, C. botulinum, and C. perfringens Binary Toxins. *Biophys. J.* **2012**, *103*, 1208−1217.
(36) Kasianowicz, J. J.; Bezrukov, S. M. Protonation dynamics of the alpha-toxin ion channel from spectral analysis of pH-dependent current fluctuations. *Biophys. J.* **1995**, *69*, 94−105.
(37) Nestorovich, E. M.; Karginov, V. A.; Bezrukov, S. M. Polymer partitioning and ion selectivity suggest asymmetrical shape for the membrane pore formed by epsilon toxin. *Biophys. J.* **2010**, *99*, 782−789.
(38) Neumeyer, T.; Schiffler, B.; Maier, E.; Lang, A. E.; Aktories, K.; Benz, R. Clostridium botulinum C2 toxin. Identification of the binding site for chloroquine and related compounds and influence of the binding site on properties of the C2II channel. *J. Biol. Chem.* **2008**, *283*, 3904−3914.
(39) Knapp, O.; Maier, E.; Waltenberger, E.; Mazuet, C.; Benz, R.; Popoff, M. R. Residues involved in the pore-forming activity of the Clostridium perfringens iota toxin. *Cell. Microbiol.* **2015**, *17*, 288−302.
(40) Yamada, T.; Yoshida, T.; Kawamoto, A.; Mitsuoka, K.; Iwasaki, K.; Tsuge, H. Cryo-EM structures reveal translocational unfolding in the clostridial binary iota toxin complex. *Nat. Struct. Mol. Biol.* **2020**, 288.
(41) Bendat, J. S.; Piersol, A. G. *Random data : analysis and measurement procedures*. 4th ed. ed.; Wiley: Hoboken, N. J., 2010.
(42) Yamini, G.; Nestorovich, E. M. Relevance of the alternate conductance states of anthrax toxin channel. *Proc. Natl. Acad. Sci. U. S. A.* **2017**, *114*, E2545−E2546.
(43) Kalu, N.; Alcaraz, A.; Yamini, G.; Abolfath, S. M.; Lucas, L.; Kenney, C.; Aguilella, V. M.; Nestorovich, E. M. Effect of Endosomal Acidification on Small Ion Transport through the Anthrax Toxin PA_{63} Channel. *FEBS Lett.* **2017**, *591*, 3481−3492.
(44) Kintzer, A. F.; Thoren, K. L.; Sterling, H. J.; Dong, K. C.; Feld, G. K.; Tang, I. I.; Zhang, T. T.; Williams, E. R.; Berger, J. M.; Krantz, B. A. The protective antigen component of anthrax toxin forms functional octameric complexes. *J. Mol. Biol.* **2009**, *392*, 614−629.
(45) Phillips, D. D.; Fattah, R. J.; Crown, D.; Zhang, Y.; Liu, S.; Moayeri, M.; Fischer, E. R.; Hansen, B. T.; Ghirlando, R.; Nestorovich, E. M.; Wein, A. N.; Simons, L.; Leppla, S. H.; Leysath, C. E. Engineering anthrax toxin variants that exclusively form octamers and their application to targeting tumors. *J. Biol. Chem.* **2013**, *288*, 9058−9065.
(46) Petosa, C.; Collier, R. J.; Klimpel, K. R.; Leppla, S. H.; Liddington, R. C. Crystal structure of the anthrax toxin protective antigen. *Nature* **1997**, *385*, 833−838.

https://doi.org/10.1021/acs.jpcb.0c10490
J. Phys. Chem. B 2021, 125, 5466−5478

(47) Kalu, N.; Atsmon-Raz, Y.; Momben Abolfath, S.; Lucas, L.; Kenney, C.; Leppla, S. H.; Tieleman, D. P.; Nestorovich, E. M. Effect of late endosomal DOBMP lipid and traditional model lipids of electrophysiology on the anthrax toxin channel activity. *Biochim. Biophys. Acta* **2018**, *1860*, 2192−2203.
(48) Das, D.; Krantz, B. A. Peptide- and proton-driven allosteric clamps catalyze anthrax toxin translocation across membranes. *Proc. Natl. Acad. Sci. U. S. A.* **2016**, *113*, 9611−9616.
(49) Nestorovich, E. M.; Rostovtseva, T. K.; Bezrukov, S. M. Residue ionization and ion transport through OmpF channels. *Biophys. J.* **2003**, *85*, 3718−3729.
(50) Nestorovich, E. M.; Danelon, C.; Winterhalter, M.; Bezrukov, S. M. Designed to penetrate: time-resolved interaction of single antibiotic molecules with bacterial pores. *Proc. Natl. Acad. Sci. U. S. A.* **2002**, *99*, 9789−9794.
(51) Rostovtseva, T. K.; Bezrukov, S. M. ATP transport through a single mitochondrial channel, VDAC, studied by current fluctuation analysis. *Biophys. J.* **1998**, *74*, 2365−2373.
(52) Aryal, P.; Abd-Wahab, F.; Bucci, G.; Sansom, M. S. P.; Tucker, S. J. A hydrophobic barrier deep within the inner pore of the TWIK-1 K2P potassium channel. *Nat. Commun.* **2014**, *5*, 4377.
(53) Blaustein, R. O.; Lea, E. J.; Finkelstein, A. Voltage-dependent block of anthrax toxin channels in planar phospholipid bilayer membranes by symmetric tetraalkylammonium ions. Single-channel analysis. *J. Gen. Phys.* **1990**, *96*, 921−942.
(54) Bachran, C.; Leppla, S. H. Tumor Targeting and Drug Delivery by Anthrax Toxin. *Toxins* **2016**, *8*, 197.
(55) Humphrey, W.; Dalke, A.; Schulten, K. VMD: visual molecular dynamics. *J. Mol. Graph.* **1996**, *14*, 33−38 27-8.
(56) Blaustein, R. O.; Koehler, T. M.; Collier, R. J.; Finkelstein, A. Anthrax toxin: channel-forming activity of protective antigen in planar phospholipid bilayers. *Proc. Natl. Acad. Sci. U. S. A.* **1989**, *86*, 2209−2213.
(57) Aksimentiev, A.; Schulten, K. Imaging α-hemolysin with molecular dynamics: ionic conductance, osmotic permeability, and the electrostatic potential map. *Biophys. J.* **2005**, *88*, 3745−3761.
(58) Mandal, T.; Kanchi, S.; Ayappa, K. G.; Maiti, P. K. pH controlled gating of toxic protein pores by dendrimers. *Nanoscale* **2016**, *8*, 13045−13058.
(59) Rao, S.; Lynch, C. I.; Klesse, G.; Oakley, G. E.; Stansfeld, P. J.; Tucker, S. J.; Sansom, M. S. P. Water and hydrophobic gates in ion channels and nanopores. *Faraday Discuss.* **2018**, *209*, 231−247.
(60) Jensen, M. O.; Borhani, D. W.; Lindorff-Larsen, K.; Maragakis, P.; Jogini, V.; Eastwood, M. P.; Dror, R. O.; Shaw, D. E. Principles of conduction and hydrophobic gating in K^+ channels. *Proc. Natl. Acad. Sci. U. S. A.* **2010**, *107*, 5833−5838.
(61) Anishkin, A.; Akitake, B.; Kamaraju, K.; Chiang, C. S.; Sukharev, S. Hydration properties of mechanosensitive channel pores define the energetics of gating. *J. Phys. Condens. Matter : Inst. Phys. J.* **2010**, *22*, 454120.
(62) Dong, H.; Fiorin, G.; Carnevale, V.; Treptow, W.; Klein, M. L. Pore waters regulate ion permeation in a calcium release-activated calcium channel. *Proc. Natl. Acad. Sci. U. S. A.* **2013**, *110*, 17332−17337.
(63) Nordin, N.; Guskov, A.; Phua, T.; Sahaf, N.; Xia, Y.; Lu, S.; Eshaghi, H.; Eshaghi, S. Exploring the structure and function of Thermotoga maritima CorA reveals the mechanism of gating and ion selectivity in Co^{2+}/Mg^{2+} transport. *Biochem. J.* **2013**, *451*, 365−374.
(64) Yamashita, M.; Yeung, P. S. W.; Ing, C. E.; McNally, B. A.; Pomès, R.; Prakriya, M. STIM1 activates CRAC channels through rotation of the pore helix to open a hydrophobic gate. *Nat. Commun.* **2017**, *8*, 14512−14512.
(65) Jia, Z.; Yazdani, M.; Zhang, G.; Cui, J.; Chen, J. Hydrophobic gating in BK channels. *Nat. Commun.* **2018**, *9*, 3408−3408.
(66) Zheng, W.; Hu, R.; Cai, R.; Hofmann, L.; Hu, Q.; Fatehi, M.; Long, W.; Kong, T.; Tang, J.; Light, P.; Flockerzi, V.; Cao, Y.; Chen, X. Z. Identification and characterization of hydrophobic gate residues in TRP channels. *FASEB J.* **2018**, *32*, 639−653.
(67) Machen, A. J.; Fisher, M. T.; Freudenthal, B. D., Caught in the Act: Anthrax Toxin Translocation Complex Reveals insight into the Lethal Factor Unfolding and Refolding mechanism. *bioRxiv* **2020**, 2020.04.20.049601.
(68) Gonti, S.; Westler, W. M.; Miyagi, M.; Bann, J. G. Site-Specific Labeling and (19)F NMR Provide Direct Evidence for Dynamic Behavior of the Anthrax Toxin Pore ϕ-Clamp Structure. *Biochemistry* **2021**, 643.
(69) Zorkot, M.; Golestanian, R.; Bonthuis, D. J. The Power Spectrum of Ionic Nanopore Currents: The Role of Ion Correlations. *Nano Lett.* **2016**, *16*, 2205−2212.
(70) Tasserit, C.; Koutsioubas, A.; Lairez, D.; Zalczer, G.; Clochard, M. C. Pink noise of ionic conductance through single artificial nanopores revisited. *Phys. Rev. Lett.* **2010**, *105*, 260602.
(71) Scott, C. C.; Gruenberg, J. Ion flux and the function of endosomes and lysosomes: pH is just the start: the flux of ions across endosomal membranes influences endosome function not only through regulation of the luminal pH. *BioEssays* **2011**, *33*, 103−110.
(72) Panchal, R. G.; Halverson, K. M.; Ribot, W.; Lane, D.; Kenny, T.; Abshire, T. G.; Ezzell, J. W.; Hoover, T. A.; Powell, B.; Little, S.; Kasianowicz, J. J.; Bavari, S. Purified Bacillus anthracis lethal toxin complex formed in vitro and during infection exhibits functional and biological activity. *J. Biol. Chem.* **2005**, *280*, 10834−10839.
(73) Shozeb, H.; Benjamin, A. H.; Mark, S. P. S. Simulations of a Protein Translocation Pore: SecY. *Biochemistry* **2006**, 13018.
(74) Melnyk, R. A.; Collier, R. J. A loop network within the anthrax toxin pore positions the phenylalanine clamp in an active conformation. *Proc. Natl. Acad. Sci. U. S. A.* **2006**, *103*, 9802−9807.
(75) Thoren, K. L.; Worden, E. J.; Yassif, J. M.; Krantz, B. A. Lethal factor unfolding is the most force-dependent step of anthrax toxin translocation. *Proc. Natl. Acad. Sci. U. S. A.* **2009**, *106*, 21555−21560.
(76) Hua, L.; Huang, X.; Liu, P.; Zhou, R.; Berne, B. J. Nanoscale dewetting transition in protein complex folding. *J. Phys. Chem. B* **2007**, *111*, 9069−9077.
(77) Krantz, B. A.; Finkelstein, A.; Collier, R. J. Protein translocation through the anthrax toxin transmembrane pore is driven by a proton gradient. *J. Mol. Biol.* **2006**, *355*, 968−979.
(78) Pomerantsev, A. P.; McCall, R. M.; Chahoud, M.; Hepler, N. K.; Fattah, R.; Leppla, S. H. Genome engineering in Bacillus anthracis using tyrosine site-specific recombinases. *PLoS One* **2017**, *12*, No. e0183346.
(79) Klimpel, K. R.; Molloy, S. S.; Thomas, G.; Leppla, S. H. Anthrax toxin protective antigen is activated by a cell surface protease with the sequence specificity and catalytic properties of furin. *Proc. Natl. Acad. Sci. U. S. A.* **1992**, *89*, 10277−10281.
(80) Montal, M.; Mueller, P. Formation of bimolecular membranes from lipid monolayers and a study of their electrical properties. *Proc. Natl. Acad. Sci. U. S. A.* **1972**, *69*, 3561−3566.
(81) Jo, S.; Lim, J. B.; Klauda, J. B.; Im, W. CHARMM-GUI Membrane Builder for mixed bilayers and its application to yeast membranes. *Biophys. J.* **2009**, *97*, 50−58.
(82) Lee, K. I.; Jo, S.; Rui, H.; Egwolf, B.; Roux, B.; Pastor, R. W.; Im, W. Web interface for Brownian dynamics simulation of ion transport and its applications to beta-barrel pores. *J. Comput. Chem.* **2012**, *33*, 331−339.
(83) Case, D. A.; Cheatham, T. E., III; Darden, T.; Gohlke, H.; Luo, R.; Merz, K. M., Jr.; Onufriev, A.; Simmerling, C.; Wang, B.; Woods, R. J. The Amber biomolecular simulation programs. *J. Comput. Chem.* **2005**, *26*, 1668−1688.
(84) Pearlman, D. A.; Case, D. A.; Caldwell, J. W.; Ross, W. S.; Cheatham, T. E.; DeBolt, S.; Ferguson, D.; Seibel, G.; Kollman, P. AMBER, a package of computer programs for applying molecular mechanics, normal mode analysis, molecular dynamics and free energy calculations to simulate the structural and energetic properties of molecules. *Comput. Phys. Commun.* **1995**, *91*, 1−41.
(85) Dickson, C. J.; Madej, B. D.; Skjevik, Å. A.; Betz, R. M.; Teigen, K.; Gould, I. R.; Walker, R. C. Lipid14: The Amber Lipid Force Field. *J. Chem. Theory Comput.* **2014**, *10*, 865−879.

https://doi.org/10.1021/acs.jpcb.0c10490
J. Phys. Chem. B 2021, 125, 5466−5478

(86) Maier, J. A.; Martinez, C.; Kasavajhala, K.; Wickstrom, L.; Hauser, K. E.; Simmerling, C. ff14SB: Improving the Accuracy of Protein Side Chain and Backbone Parameters from ff99SB. *J. Chem. Theory Comput.* **2015**, *11*, 3696−3713.
(87) Darden, T.; York, D.; Pedersen, L. Particle mesh Ewald: An N·log(N) method for Ewald sums in large systems. *J. Chem. Phys.* **1993**, *98*, 10089−10092.
(88) Ryckaert, J.-P.; Ciccotti, G.; Berendsen, H. J. C. Numerical integration of the cartesian equations of motion of a system with constraints: molecular dynamics of n-alkanes. *J. Comput. Phys.* **1977**, *23*, 327−341.
(89) Kanchi, S.; Suresh, G.; Priyakumar, U. D.; Ayappa, K. G.; Maiti, P. K. Molecular Dynamics Study of the Structure, Flexibility, and Hydrophilicity of PETIM Dendrimers: A Comparison with PAMAM Dendrimers. *J. Phys. Chem. B* **2015**, *119*, 12990−13001.
(90) Bhattacharya, R.; Kanchi, S.; C, R.; Lakshminarayanan, A.; Seeck, O. H.; Maiti, P. K.; Ayappa, K. G.; Jayaraman, N.; Basu, J. K. A new microscopic insight into membrane penetration and reorganization by PETIM dendrimers. *Soft Matter* **2014**, *10*, 7577−7587.
(91) Kanchi, S.; Gosika, M.; Ayappa, K. G.; Maiti, P. K. Dendrimer Interactions with Lipid Bilayer: Comparison of Force Field and Effect of Implicit vs Explicit Solvation. *J. Chem. Theory Comput.* **2018**, *14*, 3825−3839.
(92) Sahoo, A. K.; Kanchi, S.; Mandal, T.; Dasgupta, C.; Maiti, P. K. Translocation of Bioactive Molecules through Carbon Nanotubes Embedded in the Lipid Membrane. *ACS Appl. Mater. Interfaces* **2018**, *10*, 6168−6179.
(93) Majhi, A. K.; Kanchi, S.; Venkataraman, V.; Ayappa, K. G.; Maiti, P. K. Estimation of activation energy for electroporation and pore growth rate in liquid crystalline and gel phases of lipid bilayers using molecular dynamics simulations. *Soft Matter* **2015**, *11*, 8632−8640.
(94) Desikan, R.; Maiti, P. K.; Ayappa, K. G. Assessing the structure and stability of transmembrane oligomeric intermediates of an α-helical toxin. *Langmuir* **2017**, *33*, 11496−11510.
(95) Sathyanarayana, P.; Maurya, S.; Behera, A.; Ravichandran, M.; Visweswariah, S. S.; Ayappa, K. G.; Roy, R. Cholesterol promotes cytolysin A activity by stabilizing the intermediates during pore formation. *Proc. Natl. Acad. Sci. U. S. A.* **2018**, *115*, E7323−E7330.
(96) Ponmalar, I. I.; Cheerla, R.; Ayappa, K. G.; Basu, J. K. Correlated protein conformational states and membrane dynamics during attack by pore-forming toxins. *Proc. Natl. Acad. Sci. U. S. A.* **2019**, *116*, 12839−12844.
(97) Torrie, G. M.; Valleau, J. P. Nonphysical sampling distributions in Monte Carlo free-energy estimation: Umbrella sampling. *J. Comput. Phys.* **1977**, *23*, 187−199.
(98) Roux, B. The calculation of the potential of mean force using computer simulations. *Comput. Phys. Commun.* **1995**, *91*, 275−282.
(99) Kumar, S.; Rosenberg, J. M.; Bouzida, D.; Swendsen, R. H.; Kollman, P. A. THE weighted histogram analysis method for free-energy calculations on biomolecules. I. The method. *J. Comput. Chem.* **1992**, *13*, 1011−1021.

https://doi.org/10.1021/acs.jpcb.0c10490
J. Phys. Chem. B 2021, 125, 5466−5478